ACS APPLIED NANO MATERIALS

www.acsanm.org Article

Metal Ion Sensing with Phenylenediamine Quantum Dots in Blood Serum

Landysh I. Fatkhutdinova, Hani Barhum, Elena N. Gerasimova, Mohammed Attrash, Denis S. Kolchanov, Ivan I. Vazhenin, Alexander S. Timin, Pavel Ginzburg, and Mikhail V. Zyuzin*

Cite This: *ACS Appl. Nano Mater.* 2023, 6, 23130−23141 Read Online

ACCESS | Metrics & More | Article Recommendations | Supporting Information

ABSTRACT: Among numerous optical sensing techniques, lifetime analysis of fluorescent agents has several advantages, including high responsivity to local environmental changes and reduced susceptibility to random light-scattering events during through-tissue imaging. Monitoring ion concentrations in blood vessels is among the applications for which fluorescent approaches can be particularly beneficial. However, without additional biochemical conjugation approaches, fluorescent agents lack specificity; namely, they are either weakly sensitive to salt concentrations or provide a strong nonspecific response. Here we demonstrate the efficacy of phenylenediamine carbon dots exhibiting a strong fluorescence lifetime response to the common microelements in blood such as Fe^{2+}, Fe^{3+}, and Co^{2+} ions while remaining insusceptible to Na^{2+}, Ca^{2+}, Mn^{2+}, Mg^{2+}, Zn^{2+}, and Ni^{2+} ions. The paper also discusses the physical mechanisms underlying the observed selective sensitivity of the obtained CDs. Sensing performances of the carbon dots were also demonstrated with model cells on pathways to *in vivo* applications.

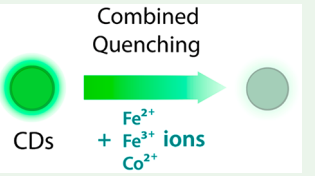

KEYWORDS: *carbon dots, quenching mechanism, metal ion detection, sensors, blood microelements*

INTRODUCTION

Microelements dissolved in the bloodstream are essential in various physiological functions. For instance, ferrous ions (Fe^{2+}) are found in hemoglobin and have a central role in oxygen transport through the bloodstream. Furthermore, Fe^{2+} ions are crucial in hematopoiesis (the formation of blood cellular components), transportation of molecules, and nutrient distribution in the body.[1] Lack of these ions in the blood leads to deficiency anemia,[2] whereas an increased level is defined as hemochromatosis, which might lead to organ dysfunction. Furthermore, elevated levels of these ions can lead to a buildup of reactive oxygen species and radicals and eventually to ischemic damage.[3] Another essential element is cobalt (Co^{2+}), a component of the water-soluble complex Cobalamin (Vitamin B-12),[4] which is crucial for various metabolic processes. For instance, it reduces the homocysteine level, thus protecting the heart and blood vessels. Furthermore, Cobalamin participates in the division and formation of blood cells and is essential for normal nervous system functioning. While a deficiency in Vitamin B-12 can lead to anemia, its excess can cause asthma, rhinitis, and cardiomyopathy.[5,6] Therefore, given their vital biological functions, selective detection of environmentally significant metal ions, specifically Fe^{2+} and Co^{2+}, is critical for health monitoring and maintaining normal bodily functions.

There are a variety of approaches for qualitative and quantitative detection of metal ions, including atomic absorption spectrophotometry,[7] inductively coupled plasma mass spectroscopy,[8] Auger electron spectroscopy,[9] chemiluminescence,[10] and several others. All of the mentioned methods require sophisticated equipment and skilled personnel. Being time-consuming, these approaches also cannot be considered for *in situ* monitoring. As an alternative, spectroscopic techniques are being explored, as they offer a faster response and reasonable sensitivity, which makes them a suitable technological compromise.[11,12] Indeed, several optically responsive nanomaterials such as quantum dots, plasmonic nanoparticles, and fluorescent polymer dots were reported to effectively detect biological molecules.[13−16] Among various fluorescent nanomaterials, carbon dots (CDs) have demonstrated potential as sensing agents of metal ions due to their low photobleaching and good water solubility.[12,17−19] For example, it was revealed that fluorescent CDs can be used for the detection of Pd^{2+}, Hg^{2+}, Fe^{2+}, and others.[20−26] The response of CDs to metal ions is generally monitored by measuring their fluorescence intensity. Furthermore, there are reports on fluorophore lifetime measurements for ion sensing. For example, a biosensor was reported using turquoise fluorescence lifetime for the detection of Ca^{2+} ions inside living cells.[27] A functionalized iridium(III) lifetime sensor was demonstrated to detect phosphate ions (PO_4^{3-}). However, to elucidate the fluorescence mechanisms (e.g., static or dynamic

Received: September 20, 2023
Revised: November 4, 2023
Accepted: November 13, 2023
Published: December 5, 2023

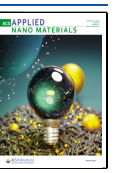

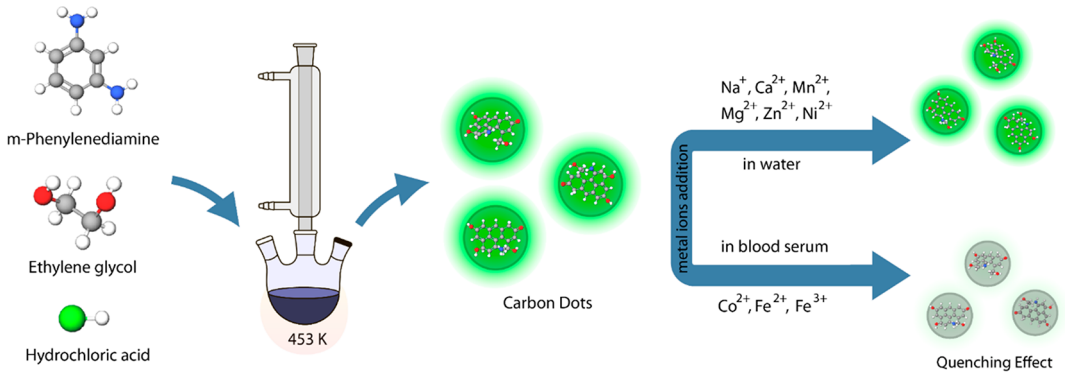

Figure 1. Schematic illustration of the performed study, including the synthesis procedure of CDs and their optical responses to metal ions.

quenching) in the presence of metal ions, both fluorescence intensity and lifetime measurements should be performed.

Thus, we investigate the optical sensing capabilities of synthesized *m*-phenylenediamine CDs by mixing them with different metal ions to achieve specificity. The CDs synthesized from phenylenediamine were selected due to their inherent sensitivity and affinity to metal ions at picomolar levels, as established in our preliminary investigations.[28,29] We demonstrate that the developed CDs possess pronounced sensitivities to Fe^{2+}, Fe^{3+}, and Co^{2+}. It is of interest to note that in terms of optical response our CDs are less sensitive to metal ions, including Na^{2+}, Ca^{2+}, Mn^{2+}, Mg^{2+}, Zn^{2+}, and Ni^{2+} (Figure 1). Furthermore, the underlying mechanisms of this selective sensing are investigated. Additional tests are also performed in blood serum, verifying the concept. These special properties of CDs could be further utilized to develop a selective detection mechanism for Fe^{2+}, Fe^{3+}, and Co^{2+}, thus contributing to advances in medical diagnostics and environmental monitoring.

EXPERIMENTAL SECTION

Materials. *m*-Phenylenediamine, ethylene glycol, hydrochloric acid, sodium chloride (NaCl), calcium chloride ($CaCl_2$), manganese chloride ($MnCl_2$), magnesium chloride ($MgCl_2$), zinc chloride ($ZnCl_2$), nickel(II) chloride ($NiCl_2$), iron(II) chloride ($FeCl_2$), cobaltous chloride ($CoCl_2$), and iron(III) chloride ($FeCl_3$) were purchased from Sigma-Aldrich (Merck Ltd.). Alpha Minimum Essential Medium (Alpha-MEM) was purchased from Biolot, Russia. Phosphate-buffered saline (PBS) and UltraGlutamine I were purchased from Lonza, Switzerland. Fetal bovine serum (FBS) was obtained from HyClone, USA. Trypsin−EDTA solution was purchased from Capricorn Scientific, Germany. Rhodamine 800 (Rh800, ≥95%) was purchased from Sigma-Aldrich.

Synthesis of CDs. Luminescent carbon dots (CDs) were synthesized using *m*-phenylenediamine (mPD) as the carbon source.[30,31] The complete experimental details can be found in our previous work.[32] Briefly, the synthesis involved a solvothermal reaction conducted in an ethylene glycol environment acidified with hydrochloric acid. To initiate the process, 95 mL of ethylene glycol and 5 mL of concentrated HCl were heated to 453 K in a three-necked flask. Subsequently, 1 g of mPD was introduced into the reaction, and the solution was refluxed for 3 h.

Following the reflux, the resulting dark solution was cooled to ambient temperature. The next phase involved blending the carbonization extract with acetonitrile in a 1:5 ratio, followed by centrifugation at 5000 rpm for 30 min. The supernatant was decanted into a 100 mL beaker and then evaporated by heating to 353 K. The residual dark colloid containing the CDs was dried on a glass slide and subsequently rinsed into a 100 mL beaker with ethanol. Afterward, the obtained CDs were dried overnight in a vacuum chamber. The final purification steps were repeated to achieve the highest-purity CDs for further study. The CDs from the initial solution were rendered usable following 30 min of centrifugation.

Structure Characterization. Transmission electron microscopy (TEM, Jeol JEM 1011, Japan) was used to characterize the morphology of the CDs. A Vertex 70 spectrophotometer (Bruker) was used for Fourier transform infrared spectroscopy (FT-IR). A Canning 5600 AES/XPS multitechnique system (PHI, USA) was used for X-ray photoelectron spectroscopy (XPS). For fluorescence and absorbance measurements, a Horiba Jobin Yvon FL3-11 spectrofluorometer was used. A Photocor Complex (Photocor, Russia) was used to investigate the CDs' size distribution.

Detection of the Metal Ions. To detect metal ions, aqueous solutions of NaCl, $CaCl_2$, $MnCl_2$, $MgCl_2$, $ZnCl_2$, $NiCl_2$, $FeCl_2$, $FeCl_3$, and $CoCl_2$ with different concentrations (10^{-4}−1 mM) were added into a 2 mL CDs solution (0.01 mg/mL) in a cuvette. Fluorescence emission spectra were observed for each sample, with varying intensities recorded at 530 nm upon 450 nm excitation.

For lifetime decay measurements in aqueous solutions and in blood serum, the time-correlated single photon counting (TCSPC) method was introduced. For CDs excitation, we applied a 405 nm wavelength diode laser (LDH-P-C-405 M head, Piqoquant). During the measurements, CD solutions in water or blood serum were dropped on a microscope slide and then covered with an additional coverslip to prevent liquid evaporation. The experimental details are described in the Supporting Information.

Cell Culture. B16-F10 cells were obtained from the American Type Culture Collection and were cultured with AlphaMEM supplemented with 10 vol % of fetal bovine serum at 37 °C.

Cell Cytotoxicity. The toxicity of CDs was estimated using the alamarBlue assay. To do that first, B16-F10 cells were seeded in a 96-well plate. The next day, various amounts of CDs were added to the cells, and the cells were left overnight. Then, the cell medium was removed and replaced with a cell culture medium supplemented with 10 vol % of alamarBlue. Then, the cells were incubated for 4 h. The cell viability was estimated by measuring the absorbances at 570 and 600 nm with a UV−vis spectrophotometer (Thermo Scientific Multiskan GO). The details are presented in the Supporting Information.

Uptake Studies. To assess the cellular uptake of CDs, different amounts of CDs (100, 50, 10, 5, 1, 0.5, and 0.1 μg/mL) were incubated with B16-F10 melanoma cells. The uptake was investigated by using confocal laser scanning microscopy (CSLM). For this, the cell membranes were stained by using Rhodamine 800. The details are described in the Supporting Information.

Hemolysis Assay. A hemolysis assay was performed to study the hemolytic effect of CDs on human red blood cells (RBCs). For this, CDs (150, 100, 50, and 25 μg/mL) were mixed with RBCs. The hemoglobin content was quantitatively evaluated by using a spectrophotometer at an absorption wavelength of 540 nm. The details are presented in the Supporting Information.

https://doi.org/10.1021/acsanm.3c04494
ACS Appl. Nano Mater. 2023, 6, 23130−23141

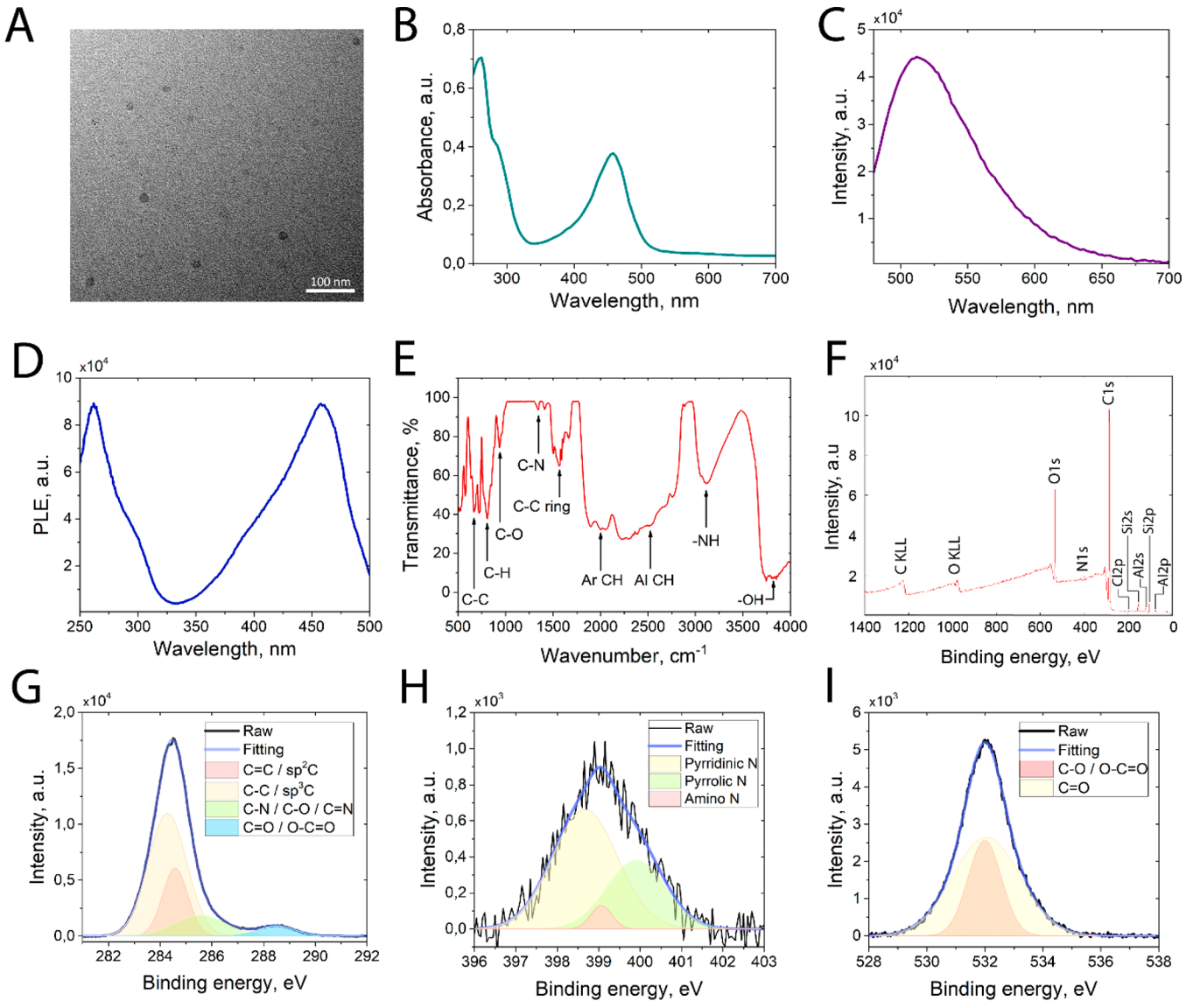

Figure 2. Characterization of mPD CDs. (A) Representative TEM image of CDs. (B) Absorbance spectrum. (C) Fluorescence spectrum for 450 nm excitation. (D) PLE spectrum acquired for CDs emitting at 530 nm. (E) FTIR spectrum with the corresponding functional groups in CDs. (F) XPS spectrum. (G) Detailed XPS spectrum for the carbon (C 1s) component. (H) Detailed XPS spectrum for the nitrogen (N 1s) component. (I) Detailed XPS spectrum for the oxygen (O 1s) component.

RESULTS AND DISCUSSION

Synthesis and Characterization of CDs. As it was mentioned above, CDs were obtained using a solvothermal synthesis approach.[32] Acetonitrile was used for an efficient dissolution of impurities, alongside ensuring fluorescent CDs remained in the solution. Upon evaporation of the solvent, we obtained a purer and more concentrated form of the fluorescent CDs. The chosen 1:5 ratio was empirically established after extensive optimization of both the fluorescence intensity and product purity. The obtained CDs' geometry, morphology, and optical properties were further investigated. Transmission electron microscopy (TEM) analysis revealed well-dispersed uniform particles with an average size of 15 ± 2 nm (Figure 2A). The absorption spectrum shown in Figure 2B demonstrates two distinct peaks located at 260 and 450 nm. The first peak, the higher and narrower one, at 260 nm is attributed to the $\pi-\pi^*$ transitions, typical for aromatic compounds, which are present in the phenylenediamine used to synthesize the CDs.[33,34] In addition, the peak at 450 nm is related to $n-\pi^*$ transitions from carboxyl groups; it might be also partially attributed to surface defects, as these functional groups are often found on the surface of CDs.[33,34] Figure 2C shows the fluorescence spectrum obtained under 450 nm excitation. The broad emission peak at 530 nm further supports the proposed absorption mechanism.[35] Furthermore, the fluorescence peak is inhomogeneously broadened due to the CDs' size variations and local environmental fluctuations in the solvent. The photoluminescence excitation (PLE) spectrum (Figure 2D) demonstrates the best excitation wavelength for the CDs to be 450 nm for emission fixed at 530 nm. It is worth noting that for CDs emitting at this wavelength, absorbances at 260 and 450 nm become equal in magnitude, suggesting a higher quantum yield (QY) for the 450 nm excitation. This could be attributed to the higher electronic density of states at the 450 nm transition, leading to a higher probability of radiative decay and

https://doi.org/10.1021/acsanm.3c04494
ACS Appl. Nano Mater. 2023, 6, 23130−23141

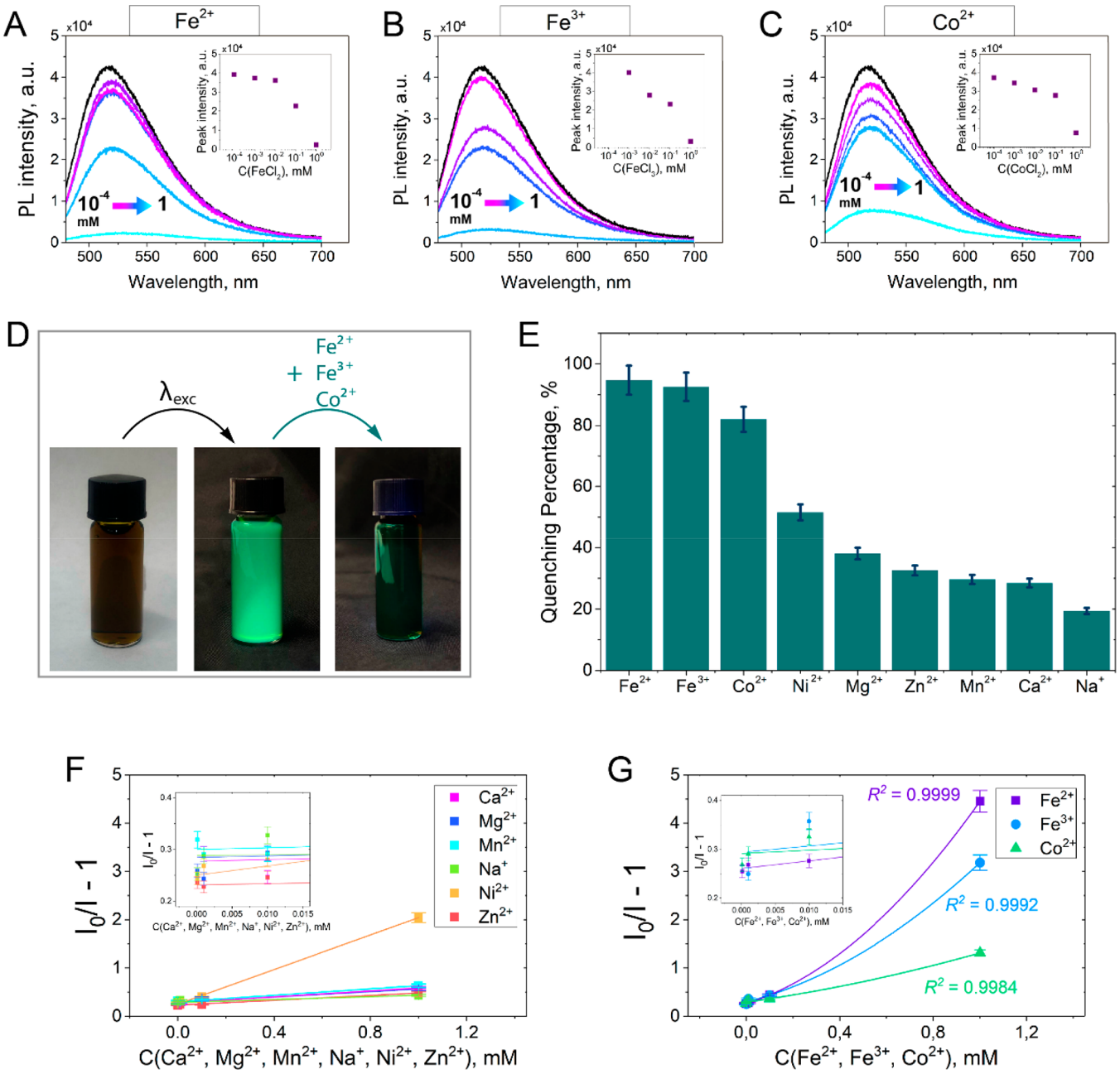

Figure 3. Fluorescence spectra (λ_{exc} = 450 nm) of mPD CDs for different concentrations of metal ions (10^{-4}–1 mM) (A) Fe^{2+}, (B) Fe^{3+}, and (C) Co^{2+}. Insets: linear relationship between the fluorescence intensity (at 530 nm) and the concentration of tested metal ions (10^{-4}–1 mM). (D) Digital image of CDs dispersed in water, which demonstrates the quenching effect upon adding Fe^{2+}, Fe^{3+}, and Co^{2+} ions. (E) Quenching percentage $[(I_0 - I)/I_0] \times 100\%$ of fluorescence intensity upon adding different metal ions (0.1 mM). Stern–Volmer plots for (F) Na^+, Ca^{2+}, Mn^{2+}, Mg^{2+}, Zn^{2+}, and Ni^{2+} and (G) Fe^{2+}, Fe^{3+}, and Co^{2+} in the concentration range 10^{-4}–1 mM.

higher rate, thereby enhancing the QY by providing more fluorescent paths for the electrons.[36]

Figure 2E presents a Fourier transform infrared (FTIR) absorption spectrum, highlighting the existence of several functional chemical groups, which can be used to further functionalize the CDs. The FTIR spectrum also contains a variety of notable peaks. The peak at 808 cm^{-1} and the peak at 937 cm^{-1} correspond to the C–H vibration and C–O stretching vibration, respectively, while the distinctive peak at 1570 cm^{-1} is related to C–C aromatic ring chain vibration. The peak at 3700 cm^{-1} is associated with the stretching of the –OH hydroxyl group, and the doublet peak close to 3100 cm^{-1} indicates the presence of the –NH and $-NH_2$ groups.[23]

Moreover, Figure S1 shows the spectrum of mPD compared with the spectrum of the obtained CDs. Peaks around 3000–3500 cm^{-1} indicate N–H stretching from the amino groups. The 1500–1600 cm^{-1} range is attributed to C=C stretching in the benzene ring. Peaks near 1300–1400 cm^{-1} suggest C–N stretching vibrations. Peaks below 1000 cm^{-1} are associated with various bending modes and specific vibrations of the benzene ring or its substituents.

To further explore the chemical composition of the synthesized CDs, we analyzed the X-ray photoelectron spectroscopy (XPS) (Figure 2F). There are three primary photoemission lines in the XPS spectrum, corresponding to C 1s (~284.5 eV), N 1s (~399 eV), and O 1s (~532 eV). The

https://doi.org/10.1021/acsanm.3c04494
ACS Appl. Nano Mater. 2023, 6, 23130–23141

presence of carbon, oxygen, and nitrogen is a cornerstone of CDs' fundamental structure.[37] The decomposed C 1s peak shows multiple subpeaks, signifying diverse carbon bonding configurations (Figure 2G). The peak located at about 284.6 eV indicates the presence of C−C sp^3 or C═C sp^2-hybridized carbon bonds. These mixed graphitic (sp^2) and aliphatic (sp^3) carbon structures reveal the composite structure of CDs, blending both aromatic and aliphatic characters. Several additional subpeaks appear around 285.6 and 286.1 eV, corresponding to C−N, C−O, and C═N bonds. The existence of these oxygen- and nitrogen-bound functional groups on the CDs' surface highlights the versatility of the surface chemistry of these nanostructures. The peak at approximately 288.5 eV indicates carboxylic acid (COOH) groups, demonstrating CDs' exceptional interfacial interaction capacity. The O 1s peak decomposition reveals another set of peaks (Figure 2H). The peak at ∼531.6 eV and the peak around 532.8−533.2 eV correspond to C═O groups and C−O bonds, respectively, which shows the contribution of the oxygen-rich groups to CDs' hydrophilicity and water stability.

The further study of the N 1s peak reveals subpeaks associated with pyridinic N (398.7 eV), pyrrolic N (399.9 eV), and graphitic N (400 eV) (Figure 2I). While pyridinic and pyrrolic nitrogen functionalities are responsible for the CDs' fluorescence, graphitic nitrogen, despite being a smaller fraction, can contribute significantly to the CDs' electronic properties by participating in the π-conjugation system. All peaks of the XPS spectrum shown in Figure 2F expose many functional groups incorporated within the synthesized CDs. The interplay of these groups is responsible for the notable properties of our CDs, such as enhanced fluorescence and high stability in water (Figure S2). To reveal the stability of CDs in water, we measured their hydrodynamic radius using a dynamic light scattering method for 2 days (Figure S3). After the measurements were performed, CDs demonstrated no significant changes in hydrodynamic diameters, which indicates their colloidal stability.

Fluorescence Intensity Response of CDs Interacting with Metal Ions. Following the discussion in the Introduction, exploring the pathways toward selective sensing of microelements is vital for health monitoring. We have analyzed the fluorescent properties of mPD CDs interacting with metal ions Na^+, Ca^{2+}, Mn^{2+}, Mg^{2+}, Zn^{2+}, Ni^{2+}, Fe^{2+}, Fe^{3+}, and Co^{2+}, in aqueous solutions first and then in blood serum. The metal ions chosen for this study, including Na^+, Ca^{2+}, Mn^{2+}, Mg^{2+}, Zn^{2+}, Ni^{2+}, Fe^{2+}, Fe^{3+}, and Co^{2+}, are prevalent in biological samples and play crucial roles in many physiological processes. Monitoring their concentrations is vital as imbalances can have significant health repercussions. Thus, our study focused on these ions to ascertain the efficacy of our CDs in detecting them in complex biological matrices. While a variety of other quenching ions exist (e.g., Hg^{2+}),[38] they have a lesser interest for biological studies. For this purpose, CDs were immersed in aqueous solutions containing metal ions at different concentrations (10^{-4}−1 mM), and their fluorescence intensity was further measured (λ_{exc} = 450 nm). This concentration range was chosen to investigate the quenching behavior in a broad range of concentrations, not only physiological ones.[29] The resulting fluorescence spectra are presented in Figures 3A−C for Fe^{2+}, Fe^{3+}, and Co^{2+} and in Figure S2 for Na^+, Ca^{2+}, Mn^{2+}, Mg^{2+}, Zn^{2+}, and Ni^{2+}. The dependencies of the fluorescence peak intensities on metal ion concentrations are shown in the insets of Figures 3A−C. According to the data obtained, the fluorescence signal intensity decreases monotonically with an increasing ion concentration. Figure 3D provides visual evidence of the measurements.

Figure 3E reveals that after adding the same concentration (0.1 mM) of different metal ions, CDs are efficiently quenched, thus serving as a sensor for detecting Fe^{2+}, Fe^{3+}, and Co^{2+}. These ions noticeably diminish the fluorescence intensity of CDs, by 94.7%, 92.3%, and 81.8%, respectively. Compared to them, other metal cations, including Na^+, Ca^{2+}, Mn^{2+}, Mg^{2+}, Zn^{2+}, and Ni^{2+}, have a much lower impact on the CDs' fluorescence, which was suppressed by approximately 40%, and in the case of Ni^{2+}, by approximately 50% (Figure 3E). Based on these findings, the CDs seem promising for a fluorescence sensor for Fe^{2+}, Fe^{3+}, and Co^{2+}.

To reveal the underlying fluorescence quenching mechanisms, the Stern−Volmer model was applied.[39] Figure 3F demonstrates Stern−Volmer plots derived from eq 1, considering Na^+, Ca^{2+}, Mn^{2+}, Mg^{2+}, Zn^{2+}, and Ni^{2+} as quenchers.

$$\frac{I_0}{I} = 1 + K_{SV}[Q] = 1 + k_q\tau_0[Q] \quad (1)$$

where I_0 and I are the fluorescence intensity of CDs in the absence and presence of a quencher, respectively, [Q] is the quencher concentration, K_{SV} is the Stern−Volmer quenching constant, k_q is the bimolecular quenching rate constant, and τ_0 is the fluorescence lifetime of CDs in the absence of a quencher.

Therefore, K_{sv} and k_q values calculated for Na^+, Ca^{2+}, Mn^{2+}, Mg^{2+}, Zn^{2+}, and Ni^{2+} are presented in Table 1. Moreover,

Table 1. Stern−Volmer Quenching Constants (K_{SV}), Bimolecular Quenching Rate Constants (k_q), and LODs for CDs in the Presence of Na^+, Ca^{2+}, Mn^{2+}, Mg^{2+}, Zn^{2+}, Ni^{2+}, Fe^{2+}, Fe^{3+}, and Co^{2+} Ions

metal ion	K_{SV}, 10^3 M^{-1}	LOD, μM	k_q, 10^8 M^{-1} s^{-1}
Na^{2+}	0.147	615.0	2.63
Ca^{2+}	0.309	238.2	5.54
Mn^{2+}	0.334	109.7	5.99
Mg^{2+}	0.280	455.6	5.02
Zn^{2+}	0.250	114.3	4.48
Ni^{2+}	1.791	27.7	32.10
Fe^{2+}	11.592	11.0	29.42
Fe^{3+}	1.642	0.7	207.75
Co^{2+}	4.961	5.3	88.90

Table 1 summarizes the estimated limits of detections (LODs) for all of the tested metal ions (LOD = $3S_d/k$, where S_d is the standard deviation for the blank solution and k is the calibration curve slope).

Note that eq 1 is valid when the experimental results exhibit a linear relationship between the fluorescence intensity and the concentration of metal ions.[39] The Stern−Volmer curves change very little for the fluorescence of CDs in the presence of Na^{2+}, Ca^{2+}, Mn^{2+}, Mg^{2+}, and Zn^{2+}, except for Ni^{2+} (Figure 3F), where K_{SV} and k_q values are an order of magnitude higher, according to the regression lines' slopes (Table 1). This indicates that in the case of Ni^{2+}, quenching is most likely caused by the collisions between CDs and Ni^{2+} ions.[40]

Among all of the metal ions tested above, only Ni^{2+} showed some detectability, although it approaches the CDs' limit of

https://doi.org/10.1021/acsanm.3c04494
ACS Appl. Nano Mater. 2023, 6, 23130−23141

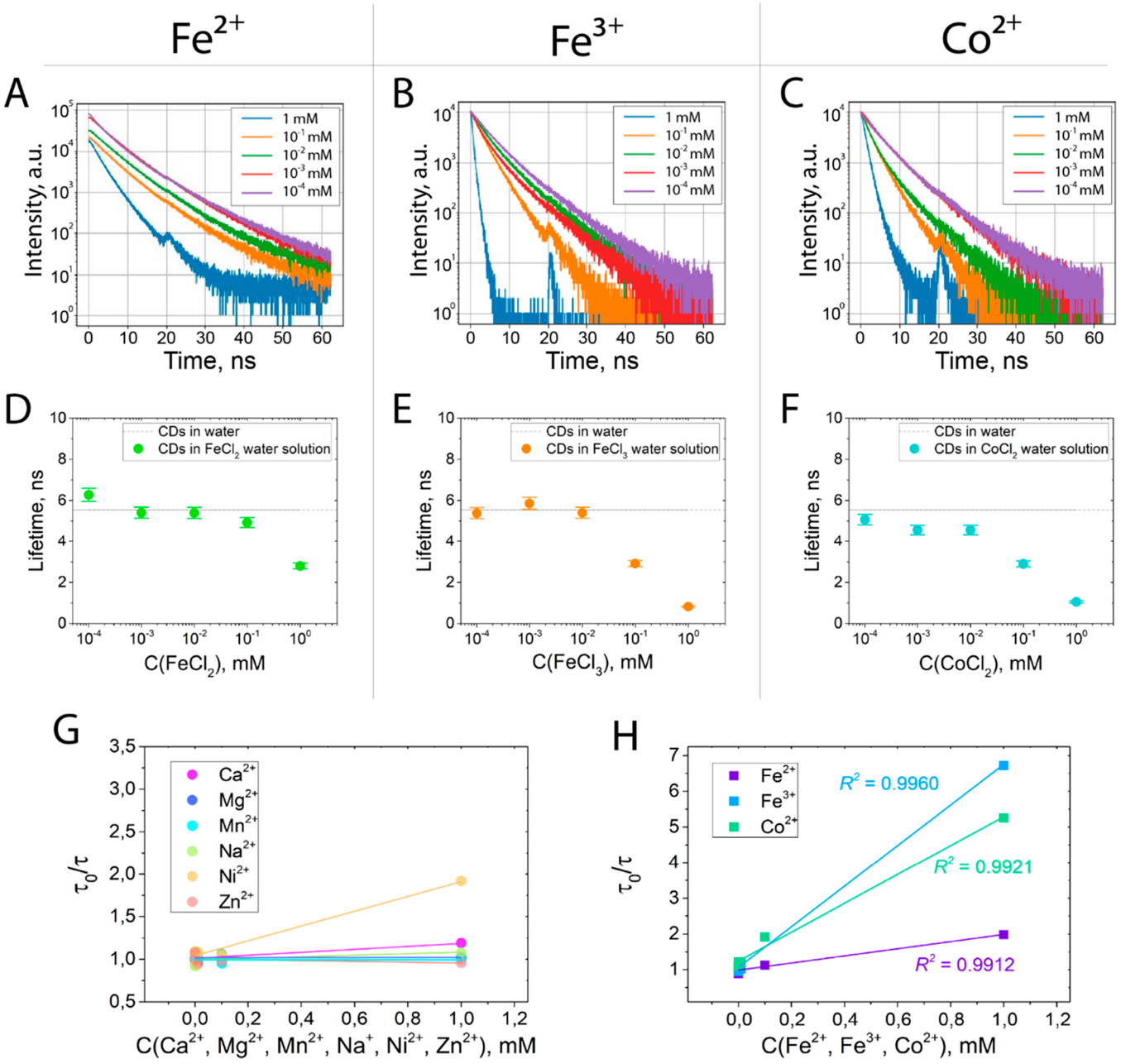

Figure 4. Lifetime spectra of CDs with ions (A) Fe^{2+}, (B) Fe^{3+}, and (C) Co^{2+} added at concentrations of 10^{-4}−1 mM. CDs' lifetime component τ_1 vs concentrations of added (D) Fe^{2+}, (E) Fe^{3+}, and (F) Co^{2+} ions dispersed in water. Stern−Volmer plots for (G) Na^+, Ca^{2+}, Mn^{2+}, Mg^{2+}, Zn^{2+}, and Ni^{2+} and (H) Fe^{2+}, Fe^{3+}, and Co^{2+} ions in the concentration range 10^{-4}−1 mM.

detection (LOD) of 27.7 μM (Table 1). It should be noted that for Ni^{2+}, k_q is equal to 32.09×10^8 M^{-1} s^{-1}, which is less than the usual value of the dynamic quenching constant not exceeding 1.00×10^{10} M^{-1} s^{-1}.[39,41] This may indicate dynamic quenching rather than static one.[42,43]

Furthermore, the observed Stern−Volmer plots for CDs upon adding Fe^{2+}, Fe^{3+}, and Co^{2+} displayed nonlinear behavior, characterized by an upward curvature (Figure 3G), which presumably indicates static quenching along with dynamic one.[40] The linear part of the calibration curve in Figure 3G was used to calculate the limit of detection for Fe^{2+}, Fe^{3+}, and Co^{2+} ions using the above-mentioned formula for the LOD. The obtained LOD values were then listed in the revised Table 1. To describe the nonlinear behavior of the Stern−Volmer plots, a modified Stern−Volmer equation (eq 2) is used, a second-order equation with respect to [Q].[44] It explains the upward curvature in the plot observed when the fluorophore is simultaneously quenched by both static and dynamic mechanisms:

$$\frac{I_0}{I} = (1 + K_{st}[Q])(1 + K_{dyn}[Q]) \quad (2)$$

The proportion of dynamic quenching in the observed decrease in fluorescence can be determined from the change in decay times, i.e., according to the dependence $\tau_0/\tau = 1 + K_{dyn}[Q]$, which will be considered below.

Lifetime Response of CDs Interacting with Metal Ions. To additionally evaluate quenching mechanisms and determine if there are dynamic processes, we performed lifetime measurements. In fact, the fluorescence lifetime is an

https://doi.org/10.1021/acsanm.3c04494
ACS Appl. Nano Mater. 2023, 6, 23130−23141

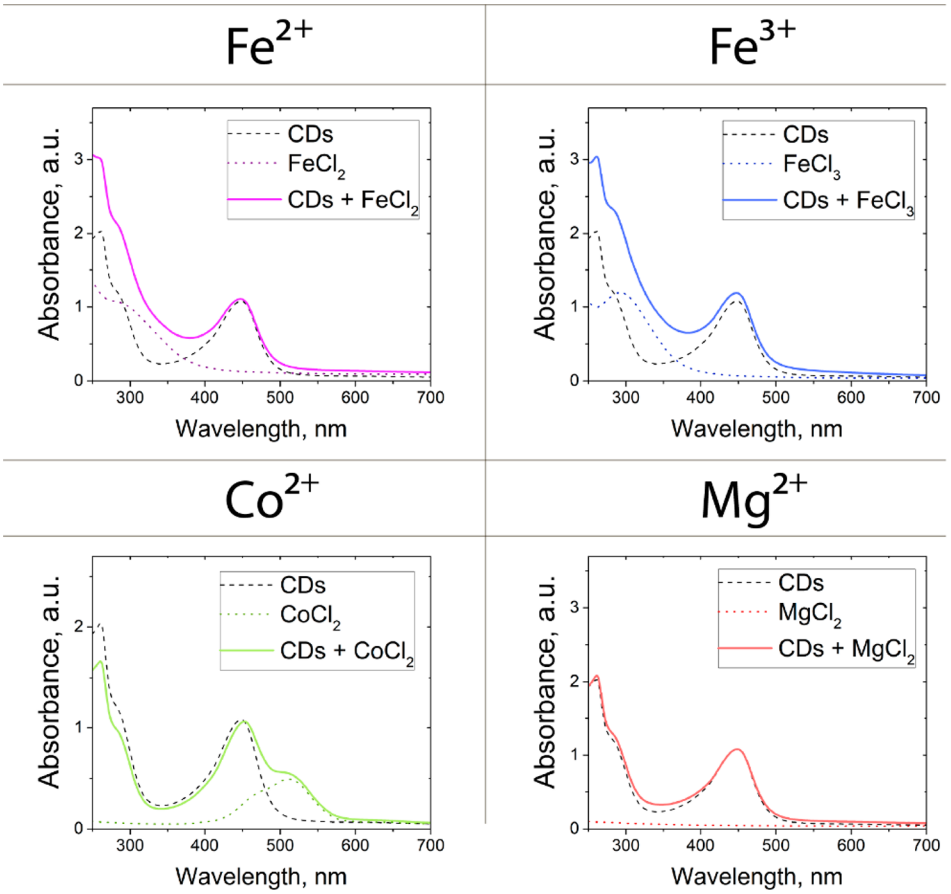

Figure 5. Absorption spectra of CDs (gray dotted lines) in the presence of $FeCl_2$ (pink), $FeCl_3$ (blue), $CoCl_2$ (green), and $MgCl_2$ (red).

intrinsic material parameter, independent of calibration and excitation source intensity fluctuations. In addition, due to the method's stability, low-intensity signals can be collected for a longer time. We measured the fluorescence lifetimes using the time-correlated single-photon counting technique (TCSPC). This method uses a series of excitation pulses with subsequent photon detection to obtain statistical properties of the decay.[45] A picosecond 405 nm diode laser (repetition rate 80 MHz) pumped the samples, and a single-photon avalanche diode (SPAD) detector was used for photon detection. The excitation wavelength is defined by the existing experimental setup and is sufficient yet not optimal for CDs' excitation. All of the measurements were performed for CDs dispersed in an aqueous solution with and without metal ions. CDs were drop-cast on a microscope slide and then covered with an additional coverslip to prevent liquid evaporation. The photon counting consisted of 64000 detections to improve the accuracy. Lifetime measurements were performed in a limited volume, which is approximately equal to the laser beam size. For each point, several lifetime measurements were performed within one sample with a relative error of 4%, which proves that the CDs and metal ions were located in close proximity to each other. Data were fitted biexponentially, relying on two characteristic times, namely, a slower component τ_1 and the faster one τ_2, which allowed a quite accurate fit. Because there are two types of CDs in the solution, i.e., the ones interacting with ions and those that are not, the two-time approximation is rather justified.[46] The fluorescence lifetimes of CDs responded weakly to Na^+, Ca^{2+}, Mn^{2+}, Mg^{2+}, Zn^{2+}, and Ni^{2+} but were significantly affected by Fe^{2+}, Fe^{3+}, and Co^{2+}, and τ_1 reduced with increasing concentrations of the latter ions. For CDs with Fe^{2+}, Fe^{3+}, and Co^{2+} ions added at concentrations of 10^{-4}–1 mM, lifetime spectra without biexponential fitting are shown in Figures 4A–C, and fitted lifetime spectra are demonstrated in Figure S4. The dependence of CDs' lifetime component τ_1 on Fe^{2+}, Fe^{3+}, and Co^{2+} ions concentrations is shown in Figures 4D–F. It is worth noting that τ_1 was found to be more responsive to the solution content and comparatively longer than τ_2.

To distinguish between dynamic and static quenching, we also studied the dependence of the excited-molecule lifetime on the quenchers' concentrations. A decrease in the lifetime of the excited molecules with increasing quencher concentration indicates a dynamic quenching mechanism, while a lifetime independent of the quencher concentration indicates predominant static quenching. Quantitatively, the static and dynamic mechanisms can be determined by comparing the dependence of the relative lifetime value of the excited molecules τ/τ_0 on the concentration of the Na^+, Ca^{2+}, Mn^{2+}, Mg^{2+}, Zn^{2+}, Ni^{2+} and Fe^{2+}, Fe^{3+}, and Co^{2+} (Figures 4G,H). In the case of Na^+, Ca^{2+}, Mn^{2+}, Mg^{2+}, and Zn^{2+}, the lifetime remains almost unchanged, similar to fluorescence measurements (Figure 4G). However, the presence of Ni^{2+} decreases both the fluorescence lifetime of CDs and their fluorescence intensity, which indicates dynamic quenching.[40] For Fe^{2+}, Fe^{3+}, and Co^{2+}, Stern–Volmer plots showed nonlinear dependencies of fluorescence and linear dependencies of relative lifetime on ion concentrations (Figure 4H). From these plots, $K_{dyn} = \tau/\tau_0 - 1$ can be calculated to estimate the dynamic quenching contribution: K_{dyn} for Fe^{2+}, Fe^{3+}, and Co^{2+} are 0.99, 5.69, and 4.04 M^{-1}, respectively.

https://doi.org/10.1021/acsanm.3c04494
ACS Appl. Nano Mater. 2023, 6, 23130–23141

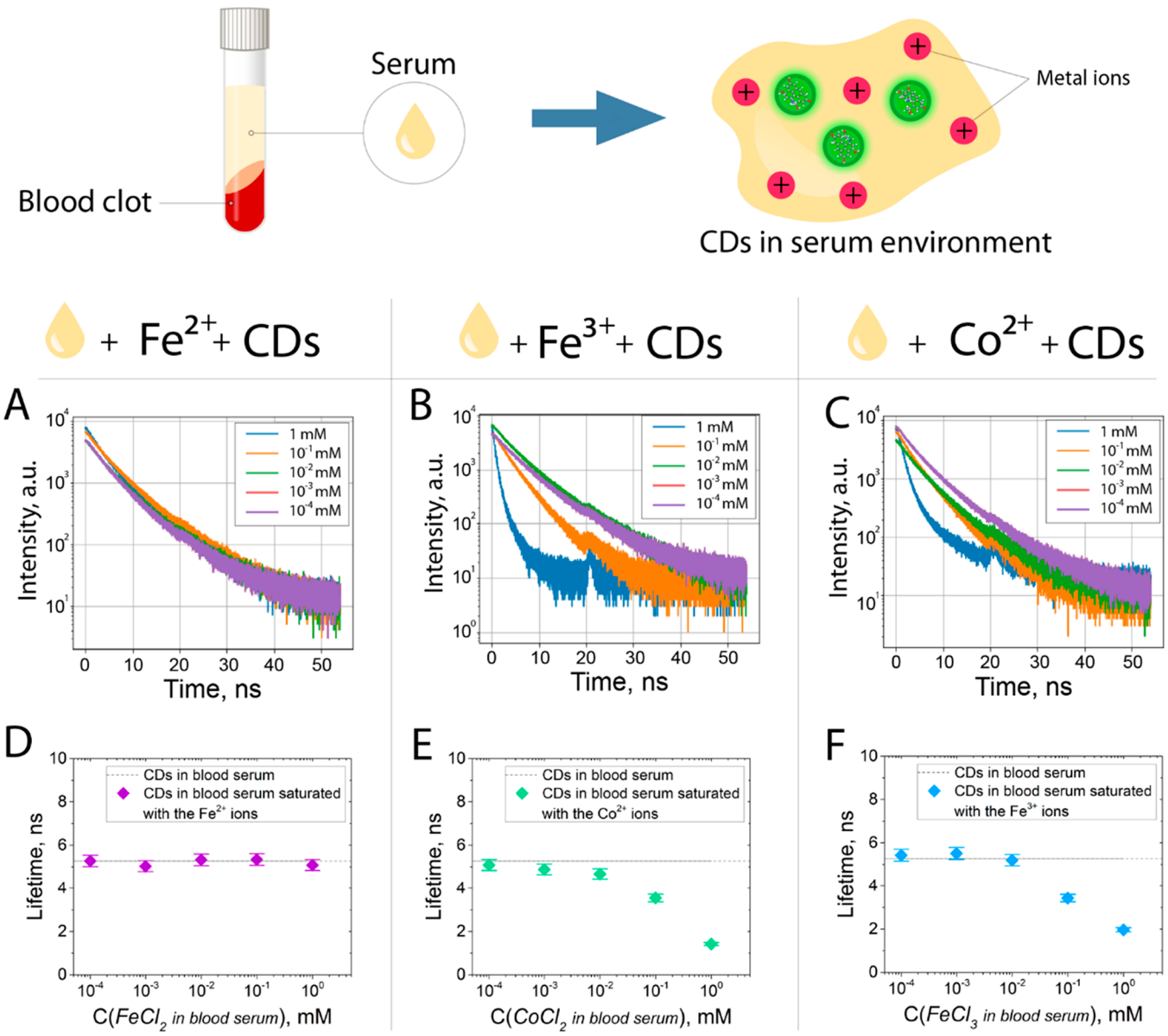

Figure 6. Upper row: schematic illustration of blood serum separation. Lifetime spectra of CDs added to (A) Fe^{2+}, (B) Fe^{3+}, and (C) Co^{2+} ions with the concentrations 10^{-4}–1 mM in blood serum. Dependence of the lifetime component τ_1 of CDs on concentrations of added (D) Fe^{2+}, (E) Fe^{3+}, and (F) Co^{2+} ions dispersed in blood serum.

Hence, in the case of CDs with Fe^{3+} and Co^{2+}, dynamic quenching is predominant due to increased slope (Figure 4H), and for CDs with Fe^{2+}, static quenching dominates.[40]

Absorption Spectra of CDs Interacting with Metal Ions. Afterward, we analyzed the CDs' absorption spectra in aqueous solutions, where there is an absorption peak at 450 nm (Figure 2B), which was attributed to CDs derived from phenylenediamines. This finding is consistent with published works,[32,47,48] in which the band gap of such carbon dots is reported to be between 2 and 3 eV. Based on our absorption spectra, we deduced a direct allowed transition with a band gap of 2.58 eV.

According to the measured absorption spectra, there was observed a slight red-shift for CDs in the presence of Fe^{2+}, Fe^{3+}, and Co^{2+} (Figure 5), which significantly affected the CDs' lifetime. For Mg^{2+}, this shift was absent, suggesting a minimal impact on the CDs' fluorescence lifetime. This phenomenon may be attributed to the chelating effect between the surface functional groups of carbon dots and metal ions. Based on IR spectroscopy, chelate complexes can be presumably formed with −NH/NH_2, −CO, and −OH groups, where nitrogen and oxygen atoms can donate lone pairs to the unoccupied orbitals of metal ions.[49] Furthermore, a detailed investigation of the absorption spectra suggests that for the Co^{2+} ion, an additional quenching mechanism should be considered, namely, the inner filter effect (IFE), stemming from a partial overlap between the Co^{2+} absorption spectrum and the CD's emission spectrum at 530 nm.[49,50]

The absorption spectra were analyzed in various solvents, including protic solvents such as water and EtOH (ethanol) and the aprotic solvent DMSO (dimethyl sulfoxide) (Figure S5). Across this solvent series, the band gap slightly decreased, which might indicate the formation of hydrogen bonds between the solvent molecules and functional groups on the CDs' surface. In subsequent studies, we plan to investigate the lifetime and emission spectra of the obtained CDs in a wide

https://doi.org/10.1021/acsanm.3c04494
ACS Appl. Nano Mater. 2023, 6, 23130−23141

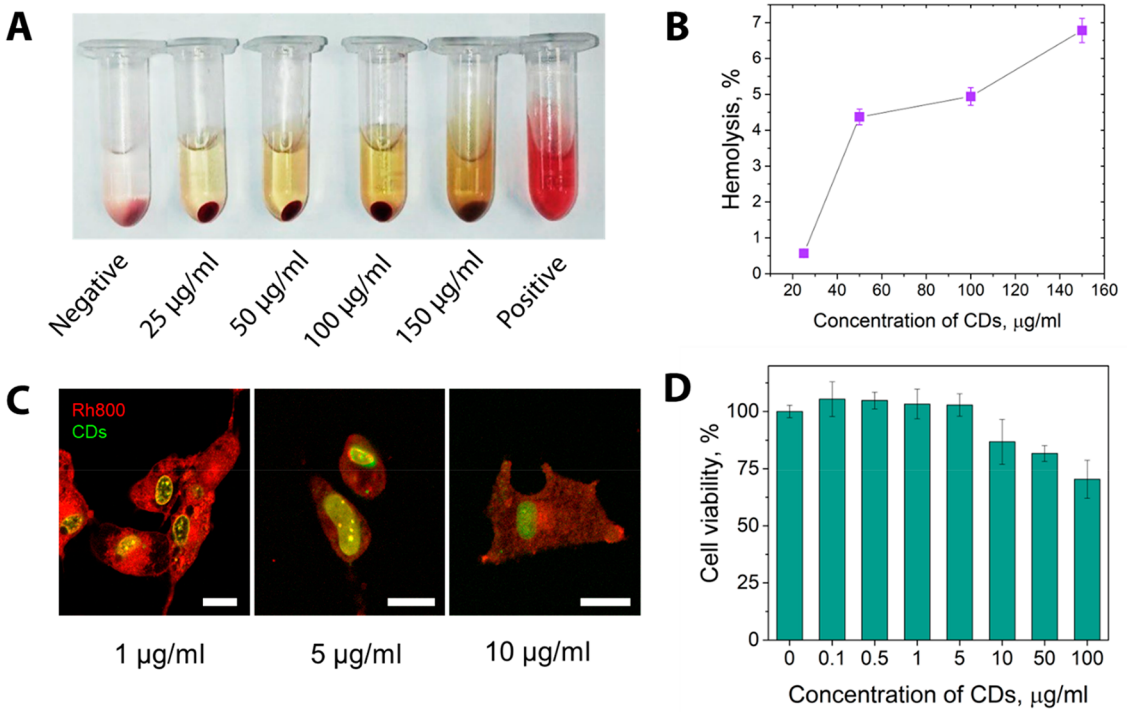

Figure 7. Cell studies. (A) Hemolysis assay depending on different concentrations of CDs. (B) Relative rate of hemolysis in human RBCs upon incubation with a suspension of MPs at different concentrations. (C) Uptake of CDs by B16-F10 cells. Cell membrane was stained using Rhodamine 800. Scale bar accounts for 25 μm. (D) Cell viability of B16-F10 cells depending on various amounts of CDs.

range of solvents. This may pave the way for enhancing the selectivity of metal ion detection and also find potential applications of CDs in optoelectronic devices and displays.

Fluorescence Lifetime Measurements of CDs Dispersed in Blood Serum. It is given that the CDs' fluorescence is affected by Fe^{2+}, Fe^{3+}, and Co^{2+} ions in aqueous solutions; thus, we measured their fluorescence lifetimes in blood serum to reveal whether a biological environment also affects them. We opted for blood serum over pure blood in our investigations, given its clinical relevance, consistency, and reduced complexity, ensuring precise and reproducible fluorescence measurements.[51,52] Similar to the previous measurements, τ_1 was plotted versus metal ion concentrations dispersed in blood serum (Figure 6). We have found that Fe^{3+} and Co^{2+} ions in blood serum influence the CDs' fluorescence lifetime similarly to those in water, but Fe^{2+} ions do not. The CDs' lifetime changes due to the presence of Fe^{2+} were less pronounced in blood serum compared to that in water solution. It has been also supposed that Fe^{2+} can be coordinated by aqua ligands in a water solution, but in blood serum, proteins can prevent the interaction between ions and CDs, which leads to the reduced effect of ions on CDs' lifetimes in blood. In addition, this could be attributed to the absence of specific binding sites for Fe^{2+} ions on the CDs surface and the difference in the electronic structure of Fe^{2+} and Fe^{3+} ions, which leads to different interactions with fluorescent CDs. Fe^{2+} ions can readily bind to oxygen and form stable complexes, preventing any interaction with CDs.[53] On the other hand, Fe^{3+} ions can easily undergo redox reactions and interact with carbon dots, leading to changes in fluorescence lifetime.[53]

This is partially true for Fe^{3+} and Co^{2+}, but the lifetime values still clearly reflect the concentration of added salts ($FeCl_3$ and $CoCl_2$). While blood serum was our primary medium for this study due to its physiological relevance, CDs can be additionally used for sensing in matrix layouts, e.g., for testing wastewater or environmental samples, where simultaneous detection of multiple ions could be of value.

Biocompatibility Evaluation of CDs. Biocompatibility of CDs was further evaluated using two different independent studies (hemolysis and viability assays). Concentrations here were chosen to comply with previous reports in the field.[54,55] The hemolysis analysis was performed to reveal the CDs' influence on the integrity of human erythrocytes. For this, CDs at different concentrations were added to isolated erythrocytes and incubated for 2 h, while lysis buffer and PBS were used as positive and negative controls, respectively. According to the data obtained, hemolysis of red blood cells increases in a dose-dependent manner with increasing CDs' concentration (Figure 7A,B). Cellular uptake of CDs was further visualized by using confocal laser scanning microscopy (CLSM). For this, the cell membranes were fluorescently stained with Rhodamine 800, and the colocalization of CDs was evaluated with z-stack CLSM images (Figure 7C). According to the images obtained, the green fluorescent signal coming from CDs was found mostly in the cell nuclei,[56] whereas red fluorescence signal originated from the stained cell membranes.

Afterward, we performed cell viability studies using a fluorescence-based resazurin test (alamarBlue assay) on model B16-F10 melanoma cells. These cells were chosen as model cells to gain additional information about the biocompatibility of CDs. The decrease of the B16-F10 cell viability was evaluated after exposure to different amounts of CDs. After 24 h, dose-dependent viability of B16-F10 cells was observed (Figure 7D). The maximal nontoxic concentration of CDs added to cells was 5 μg/mL. The further increase of the CDs' amount led to decreased cell viability (70%).

https://doi.org/10.1021/acsanm.3c04494
ACS Appl. Nano Mater. 2023, 6, 23130−23141

CONCLUSION

To summarize, we have investigated quenching mechanisms of fluorescent *m*-phenylenediamine carbon dots (CDs) upon adding metal ions Na^+, Ca^{2+}, Mn^{2+}, Mg^{2+}, Zn^{2+}, Ni^{2+}, Fe^{2+}, Fe^{3+}, and Co^{2+}. The obtained data revealed that the CDs exhibited an increased sensitivity to Fe^{2+}, Fe^{3+}, and Co^{2+} ions in terms of fluorescence intensity and fluorescence lifetime as well as almost no sensitivity to Na^+, Ca^{2+}, Mn^{2+}, Mg^{2+}, Zn^{2+}, and Ni^{2+} ions dispersed in water. Moreover, the detection of Fe^{3+} and Co^{2+} in blood serum was also achievable. The calculated quenching constants reveal that the detection of Fe^{2+}, Fe^{3+}, and Co^{2+} ions is most likely provided by a combined fluorescence quenching process. This process was combined, first, due to the complexation of CDs with Fe^{2+}, Fe^{3+}, and Co^{2+} ions and, second, because of deactivation of the excited-state fluorophore upon contact with quencher in solution (in other words, presumable collisional quenching), which is also confirmed by fluorescence lifetime measurements. Moreover, the analysis of the absorption spectra indicated a minor decrease in the band gap difference, suggesting possible hydrogen bonding between the solvent molecules and the functional groups on the carbon dots' surface. Therefore, CDs are promising for the efficient sensor platform for metal ions and a valuable tool for selective metal ion detection even in a biological environment.

ASSOCIATED CONTENT

Supporting Information

The Supporting Information is available free of charge at https://pubs.acs.org/doi/10.1021/acsanm.3c04494.

Protocol of CDs synthesis, characterization procedures of CDs, FTIR spectrum of mPD, CDs' hydrodynamic radius distribution, fluorescence spectra of CDs for different concentrations of metal ions, scheme of the lifetime measurements setup, biexponentially fitted lifetime spectra of CDs for different concentrations of metal ions, Tauc plots calculated from the absorption spectra of CDs (PDF)

AUTHOR INFORMATION

Corresponding Author

Mikhail V. Zyuzin − *School of Physics, ITMO University, 191002 St. Petersburg, Russia;* orcid.org/0000-0002-5364-2635; Email: mikhail.zyuzin@metalab.ifmo.ru

Authors

Landysh I. Fatkhutdinova − *School of Physics, ITMO University, 191002 St. Petersburg, Russia*

Hani Barhum − *Triangle Regional Research and Development Center, Kfar Qara' 3007500, Israel; Department of Electrical Engineering, Tel Aviv University, Tel Aviv 69978, Israel; Light−Matter Interaction Centre, Tel Aviv University, Tel Aviv 69978, Israel;* orcid.org/0000-0003-0214-0288

Elena N. Gerasimova − *School of Physics, ITMO University, 191002 St. Petersburg, Russia*

Mohammed Attrash − *Triangle Regional Research and Development Center, Kfar Qara' 3007500, Israel; Department of Electrical Engineering, Tel Aviv University, Tel Aviv 69978, Israel;* orcid.org/0000-0002-2500-0811

Denis S. Kolchanov − *Department of Electrical Engineering, Tel Aviv University, Tel Aviv 69978, Israel*

Ivan I. Vazhenin − *School of Physics, ITMO University, 191002 St. Petersburg, Russia*

Alexander S. Timin − *Laboratory of nano- and microencapsulation of biologically active compounds, Peter The Great St. Petersburg Polytechnic University, St. Petersburg 195251, Russian Federation;* orcid.org/0000-0002-0276-7892

Pavel Ginzburg − *Triangle Regional Research and Development Center, Kfar Qara' 3007500, Israel; Light−Matter Interaction Centre, Tel Aviv University, Tel Aviv 69978, Israel*

Complete contact information is available at: https://pubs.acs.org/10.1021/acsanm.3c04494

Author Contributions

L.I.F., H.B., and E.N.G. contributed equally to this paper.

Notes

The authors declare no competing financial interest.

ACKNOWLEDGMENTS

Part of this work related to the optical measurements was supported by the Russian Science Foundation (Project 21-72-30018); part of this work related to the characterization of nanomaterials was supported by Priority 2030 Federal Academic Leadership Program. Part of this work related to the biological experiments was supported by the Ministry of Science and Higher Education of the Russian Federation (Project No. 075-15-2021-592). The authors express their gratitude to Lydia Pogorelskaya for her proofreading of the English manuscript.

REFERENCES

(1) Venkataramani, V.Iron Homeostasis and Metabolism: Two Sides of a Coin. In *Ferroptosis: Mechanism and Diseases*; Florez, A. F., Alborzinia, H., Eds.; Advances in Experimental Medicine and Biology; Springer International Publishing: Cham, 2021; Vol. *1301*, pp 25−40.

(2) Lu, Y.; Ruan, G.; Du, W.; Li, J.; Yang, N.; Wu, Q.; Lu, L.; Zhang, C.; Li, L. Recent Progress in Rational Design of Fluorescent Probes for Fe2+ and Bioapplication. *Dyes Pigm.* **2021**, *190*, 109337.

(3) Babuponnusami, A.; Muthukumar, K. A Review on Fenton and Improvements to the Fenton Process for Wastewater Treatment. *Journal of Environmental Chemical Engineering* **2014**, *2* (1), 557−572.

(4) Abdi, Z.; Balaghi, S. E.; Sologubenko, A. S.; Willinger, M.-G.; Vandichel, M.; Shen, J.-R.; Allakhverdiev, S. I.; Patzke, G. R.; Najafpour, M. M. Understanding the Dynamics of Molecular Water Oxidation Catalysts with Liquid-Phase Transmission Electron Microscopy: The Case of Vitamin B_{12}. *ACS Sustainable Chem. Eng.* **2021**, *9* (28), 9494−9505.

(5) Bell, D. S. H. Metformin induced Vitamin B12 Deficiency Can Cause or Worsen Distal Symmetrical, Autonomic and Cardiac Neuropathy in the Patient with Diabetes. *Diabetes Obesity Metabolism* **2022**, *24* (8), 1423−1428.

(6) Umar, M.; Jahangir, N.; Faisal Khan, M.; Saeed, Z.; Sultan, F.; Sultan, A. Cobalt Cardiomyopathy in Hip Arthroplasty. *Arthroplasty Today* **2019**, *5* (3), 371−375.

(7) Malik, L. A.; Bashir, A.; Qureashi, A.; Pandith, A. H. Detection and Removal of Heavy Metal Ions: A Review. *Environ. Chem. Lett.* **2019**, *17* (4), 1495−1521.

(8) Xu, C.; He, M.; Chen, B.; Hu, B. Magnetic Porous Coordination Networks for Preconcentration of Various Metal Ions from Environmental Water Followed by Inductively Coupled Plasma Mass Spectrometry Detection. *Talanta* **2022**, *245*, 123470.

(9) Zhang, Y.; Zhai, W.; Hu, X.; Jiang, Y.; Chen, S.; Zhang, Y.; Liu, W.; Yu, Y. Application of Auger Electron Spectroscopy in Lithium-Ion

Conducting Oxide Solid Electrolytes. *Nano Res.* **2023**, *16* (3), 4039−4048.
(10) Zheng, J.; Wai, J. L.; Lake, R. J.; New, S. Y.; He, Z.; Lu, Y. DNAzyme Sensor Uses Chemiluminescence Resonance Energy Transfer for Rapid, Portable, and Ratiometric Detection of Metal Ions. *Anal. Chem.* **2021**, *93* (31), 10834−10840.
(11) Singh, P.; Singh, M. K.; Beg, Y. R.; Nishad, G. R. A Review on Spectroscopic Methods for Determination of Nitrite and Nitrate in Environmental Samples. *Talanta* **2019**, *191*, 364−381.
(12) Yarur, F.; Macairan, J.-R.; Naccache, R. Ratiometric Detection of Heavy Metal Ions Using Fluorescent Carbon Dots. *Environ. Sci.: Nano* **2019**, *6* (4), 1121−1130.
(13) Chen, S.; Liu, C.; Liu, Y.; Liu, Q.; Lu, M.; Bi, S.; Jing, Z.; Yu, Q.; Peng, W. Label Free Near Infrared Plasmonic Sensing Technique for DNA Detection at Ultralow Concentrations. *Advanced Science* **2020**, *7* (23), 2000763.
(14) Sargazi, S.; Fatima, I.; Hassan Kiani, M.; Mohammadzadeh, V.; Arshad, R.; Bilal, M.; Rahdar, A.; Díez-Pascual, A. M.; Behzadmehr, R. Fluorescent-Based Nanosensors for Selective Detection of a Wide Range of Biological Macromolecules: A Comprehensive Review. *Int. J. Biol. Macromol.* **2022**, *206*, 115−147.
(15) Cui, B.; Liu, P.; Liu, X.; Liu, S.; Zhang, Z. Molecularly Imprinted Polymers for Electrochemical Detection and Analysis: Progress and Perspectives. *Journal of Materials Research and Technology* **2020**, *9* (6), 12568−12584.
(16) Ahmadivand, A.; Gerislioglu, B. Photonic and Plasmonic Metasensors. *Laser & Photonics Reviews* **2022**, *16* (2), 2100328.
(17) Yoo, D.; Park, Y.; Cheon, B.; Park, M.-H. Carbon Dots as an Effective Fluorescent Sensing Platform for Metal Ion Detection. *Nanoscale Res. Lett.* **2019**, *14* (1), 272.
(18) Boobalan, T.; Sethupathi, M.; Sengottuvelan, N.; Kumar, P.; Balaji, P.; Gulyás, B.; Padmanabhan, P.; Selvan, S. T.; Arun, A. Mushroom-Derived Carbon Dots for Toxic Metal Ion Detection and as Antibacterial and Anticancer Agents. *ACS Appl. Nano Mater.* **2020**, *3* (6), 5910−5919.
(19) Zulfajri, M.; Gedda, G.; Chang, C.-J.; Chang, Y.-P.; Huang, G. G. Cranberry Beans Derived Carbon Dots as a Potential Fluorescence Sensor for Selective Detection of Fe^{3+} Ions in Aqueous Solution. *ACS Omega* **2019**, *4* (13), 15382−15392.
(20) Sharma, V.; Saini, A. K.; Mobin, S. M. Multicolour Fluorescent Carbon Nanoparticle Probes for Live Cell Imaging and Dual Palladium and Mercury Sensors. *J. Mater. Chem. B* **2016**, *4* (14), 2466−2476.
(21) Ren, G.; Zhang, Q.; Li, S.; Fu, S.; Chai, F.; Wang, C.; Qu, F. One Pot Synthesis of Highly Fluorescent N Doped C-Dots and Used as Fluorescent Probe Detection for Hg2+ and Ag+ in Aqueous Solution. *Sens. Actuators, B* **2017**, *243*, 244−253.
(22) Liu, F.; Jiang, Y.; Fan, C.; Zhang, L.; Hua, Y.; Zhang, C.; Song, N.; Kong, Y.; Wang, H. Fluorometric and Colorimetric Analysis of Total Iron Ions in Blood or Tap Water Using Nitrogen-Doped Carbon Dots with Tunable Fluorescence. *New J. Chem.* **2018**, *42* (12), 9676−9683.
(23) Sun, X.; Zhang, J.; Wang, X.; Zhao, J.; Pan, W.; Yu, G.; Qu, Y.; Wang, J. Colorimetric and Fluorometric Dual Mode Detection of Fe2+ in Aqueous Solution Based on a Carbon Dots/Phenanthroline System. *Arabian Journal of Chemistry* **2020**, *13* (4), 5075−5083.
(24) Mohammed, L. J.; Omer, K. M. Dual Functional Highly Luminescence B, N Co-Doped Carbon Nanodots as Nanothermometer and Fe3+/Fe2+ Sensor. *Sci. Rep* **2020**, *10* (1), 3028.
(25) Al-Jaf, S. H.; Omer, K. M. Portable Smartphone-Based Detection Integrated with Paper Based Device Functionalised with Green Emissive Carbon Dots for Selective Determination of Fe^{3+} Ions. *International Journal of Environmental Analytical Chemistry* **2022**, 1−14.
(26) Al-Jaf, S. H.; Omer, K. M. Enhancing of Detection Resolution via Designing of a Multi-Functional 3D Connector between Sampling and Detection Zones in Distance-Based Microfluidic Paper-Based Analytical Device: Multi-Channel Design for Multiplex Analysis. *Microchim Acta* **2022**, *189* (12), 482.
(27) Van Der Linden, F. H.; Mahlandt, E. K.; Arts, J. J. G.; Beumer, J.; Puschhof, J.; De Man, S. M. A.; Chertkova, A. O.; Ponsioen, B.; Clevers, H.; Van Buul, J. D.; Postma, M.; Gadella, T. W. J.; Goedhart, J. A Turquoise Fluorescence Lifetime-Based Biosensor for Quantitative Imaging of Intracellular Calcium. *Nat. Commun.* **2021**, *12* (1), 7159.
(28) Batool, M.; Junaid, H. M.; Tabassum, S.; Kanwal, F.; Abid, K.; Fatima, Z.; Shah, A. T. Metal Ion Detection by Carbon Dots—A Review. *Critical Reviews in Analytical Chemistry* **2022**, *52* (4), 756−767.
(29) Wang, Z.; Xu, C.; Lu, Y.; Chen, X.; Yuan, H.; Wei, G.; Ye, G.; Chen, J. Fluorescence Sensor Array Based on Amino Acid Derived Carbon Dots for Pattern-Based Detection of Toxic Metal Ions. *Sens. Actuators, B* **2017**, *241*, 1324−1330.
(30) Alshatteri, A. H.; Omer, K. M. Smartphone-Based Fluorescence Detection of Bilirubin Using Yellow Emissive Carbon Dots. *Anal. Methods* **2022**, *14* (17), 1730−1738.
(31) Pirot, S. M.; Omer, K. M.; Alshatteri, A. H.; Ali, G. K.; Shatery, O. B. A. Dual-Template Molecularly Surface Imprinted Polymer on Fluorescent Metal-Organic Frameworks Functionalized with Carbon Dots for Ascorbic Acid and Uric Acid Detection. *Spectrochimica Acta Part A: Molecular and Biomolecular Spectroscopy* **2023**, *291*, 122340.
(32) Barhum, H.; Alon, T.; Attrash, M.; Machnev, A.; Shishkin, I.; Ginzburg, P. Multicolor Phenylenediamine Carbon Dots for Metal-Ion Detection with Picomolar Sensitivity. *ACS Appl. Nano Mater.* **2021**, *4* (9), 9919−9931.
(33) Min, Y.-L.; Wang, T.; Zhang, Y.-G.; Chen, Y.-C. The Synthesis of Poly(p-Phenylenediamine) Microstructures without Oxidant and Their Effective Adsorption of Lead Ions. *J. Mater. Chem.* **2011**, *21* (18), 6683.
(34) Liu, Z.; Zu, Y.; Fu, Y.; Guo, S.; Zhang, Y.; Liang, H. Synthesis of Hybrid Nanostructures Composed of Copper Ions and Poly(p-Phenylenediamine) in Aqueous Solutions. *J. Nanopart. Res.* **2008**, *10* (8), 1271−1278.
(35) Zhou, Z.; Tian, P.; Liu, X.; Mei, S.; Zhou, D.; Li, D.; Jing, P.; Zhang, W.; Guo, R.; Qu, S.; Rogach, A. L. Hydrogen Peroxide-Treated Carbon Dot Phosphor with a Bathochromic-Shifted, Aggregation-Enhanced Emission for Light-Emitting Devices and Visible Light Communication. *Adv. Sci.* **2018**, *5* (8), 1800369.
(36) Jin, S.; Harris, R. D.; Lau, B.; Aruda, K. O.; Amin, V. A.; Weiss, E. A. Enhanced Rate of Radiative Decay in CdSe Quantum Dots upon Adsorption of an Exciton-Delocalizing Ligand. *Nano Lett.* **2014**, *14* (9), 5323−5328.
(37) Shim, H. S.; Kim, J. M.; Jeong, S.; Ju, Y.; Won, S. J.; Choi, J.; Nam, S.; Molla, A.; Kim, J.; Song, J. K. Distinctive Optical Transitions of Tunable Multicolor Carbon Dots. *Nanoscale Adv.* **2022**, *4* (5), 1351−1358.
(38) Choudhury, N.; Saha, B.; De, P. Recent Progress in Polymer-Based Optical Chemosensors for Cu2+ and Hg2+ Ions: A Comprehensive Review. *Eur. Polym. J.* **2021**, *145*, 110233.
(39) Yue, J.; Li, L.; Cao, L.; Zan, M.; Yang, D.; Wang, Z.; Chang, Z.; Mei, Q.; Miao, P.; Dong, W.-F. Two-Step Hydrothermal Preparation of Carbon Dots for Calcium Ion Detection. *ACS Appl. Mater. Interfaces* **2019**, *11* (47), 44566−44572.
(40) *Principles of Fluorescence Spectroscopy*; Lakowicz, J. R., Ed.; Springer US: Boston, MA, 2006.
(41) Chen, B. B.; Liu, Z. X.; Zou, H. Y.; Huang, C. Z. Highly Selective Detection of 2,4,6-Trinitrophenol by Using Newly Developed Terbium-Doped Blue Carbon Dots. *Analyst* **2016**, *141* (9), 2676−2681.
(42) Ciotta, E.; Prosposito, P.; Pizzoferrato, R. Positive Curvature in Stern-Volmer Plot Described by a Generalized Model for Static Quenching. *J. Lumin.* **2019**, *206*, 518−522.
(43) Yang, L.; Wen, J.; Li, K.; Liu, L.; Wang, W. Carbon Quantum Dots: Comprehensively Understanding of the Internal Quenching Mechanism and Application for Catechol Detection. *Sens. Actuators, B* **2021**, *333*, 129557.

https://doi.org/10.1021/acsanm.3c04494
ACS Appl. Nano Mater. 2023, 6, 23130−23141

(44) Paterson, K. A.; Arlt, J.; Jones, A. C. Dynamic and Static Quenching of 2-Aminopurine Fluorescence by the Natural DNA Nucleotides in Solution. *Methods Appl. Fluoresc.* **2020**, *8* (2), 025002.
(45) References. In *Advanced Time-Correlated Single Photon Counting Techniques*; Castleman, A. W., Toennies, J. P., Zinth, W., Eds.; Springer Series in Chemical Physics; Springer: Berlin, 2005; Vol. *81*, pp 351−387.
(46) Fitzmorris, B. C.; Pu, Y.-C.; Cooper, J. K.; Lin, Y.-F.; Hsu, Y.-J.; Li, Y.; Zhang, J. Z. Optical Properties and Exciton Dynamics of Alloyed Core/Shell/Shell $Cd_{1-x}Zn_xSe$/ZnSe/ZnS Quantum Dots. *ACS Appl. Mater. Interfaces* **2013**, *5* (8), 2893−2900.
(47) Zhao, B.; Ma, H.; Zheng, M.; Xu, K.; Zou, C.; Qu, S.; Tan, Z. Narrow bandwidth Emissive Carbon Dots: A Rising Star in the Fluorescent Material Family. *Carbon Energy* **2022**, *4* (1), 88−114.
(48) Liu, Z.; Lu, X.; Liu, M.; Wang, W. Blue, Yellow, and Red Carbon Dots from Aromatic Precursors for Light-Emitting Diodes. *Molecules* **2023**, *28* (7), 2957.
(49) Tan, Q.; Li, X.; Wang, L.; Zhao, J.; Yang, Q.; Sun, P.; Deng, Y.; Shen, G. One-Step Synthesis of Highly Fluorescent Carbon Dots as Fluorescence Sensors for the Parallel Detection of Cadmium and Mercury Ions. *Front. Chem.* **2022**, *10*, 1005231.
(50) Al-Hashimi, B.; Omer, K. M.; Rahman, H. S. Inner Filter Effect (IFE) as a Simple and Selective Sensing Platform for Detection of Tetracycline Using Milk-Based Nitrogen-Doped Carbon Nanodots as Fluorescence Probe. *Arabian Journal of Chemistry* **2020**, *13* (4), 5151−5159.
(51) Liu, P.; Li, W.; Guo, S.; Xu, D.; Wang, M.; Shi, J.; Cai, Z.; Tong, B.; Dong, Y. Application of a Novel "Turn-on" Fluorescent Material to the Detection of Aluminum Ion in Blood Serum. *ACS Appl. Mater. Interfaces* **2018**, *10* (28), 23667−23673.
(52) Karthika, A.; Selvarajan, S.; Karuppasamy, P.; Suganthi, A.; Rajarajan, M. A Novel Highly Efficient and Accurate Electrochemical Detection of Poisonous Inorganic Arsenic (III) Ions in Water and Human Blood Serum Samples Based on SrTiO3/β-Cyclodextrin Composite. *J. Phys. Chem. Solids* **2019**, *127*, 11−18.
(53) Zhang, S.-R.; Cai, S.-K.; Wang, G.-Q.; Cui, J.-Z.; Gao, C.-Z. One-Step Synthesis of N, P-Doped Carbon Quantum Dots for Selective and Sensitive Detection of Fe2+ and Fe3+ and Scale Inhibition. *J. Mol. Struct.* **2021**, *1246*, 131173.
(54) Lu, F.; Song, Y.; Huang, H.; Liu, Y.; Fu, Y.; Huang, J.; Li, H.; Qu, H.; Kang, Z. Fluorescent Carbon Dots with Tunable Negative Charges for Bio-Imaging in Bacterial Viability Assessment. *Carbon* **2017**, *120*, 95−102.
(55) Havrdova, M.; Hola, K.; Skopalik, J.; Tomankova, K.; Petr, M.; Cepe, K.; Polakova, K.; Tucek, J.; Bourlinos, A. B.; Zboril, R. Toxicity of Carbon Dots - Effect of Surface Functionalization on the Cell Viability, Reactive Oxygen Species Generation and Cell Cycle. *Carbon* **2016**, *99*, 238−248.
(56) Liu, H.; Yang, J.; Li, Z.; Xiao, L.; Aryee, A. A.; Sun, Y.; Yang, R.; Meng, H.; Qu, L.; Lin, Y.; Zhang, X. Hydrogen-Bond-Induced Emission of Carbon Dots for Wash-Free Nucleus Imaging. *Anal. Chem.* **2019**, *91* (14), 9259−9265.

https://doi.org/10.1021/acsanm.3c04494
ACS Appl. Nano Mater. 2023, 6, 23130−23141